Desalination 601 (2025) 118580

Contents lists available at ScienceDirect

Desalination

journal homepage: www.elsevier.com/locate/desal

Integrated membrane distillation-solid electrolyte-based alkaline water electrolysis for enhancing green hydrogen production

Mohammad Mahbub Kabir [a,b,c], Kwang Seop Im [d], Leonard Tijing [a,b], Yeshi Choden [a,b], Sherub Phuntsho [a,b], Md. Fazlul Karim Mamun [c], Golam Md. Sabur [c], Sang Yong Nam [d,*], Ho Kyong Shon [a,b,**]

[a] ARC Research Hub for Nutrients in a Circular Economy, School of Civil and Environmental Engineering, Faculty of Engineering and Information Technology, University of Technology Sydney, 15 Broadway, NSW 2007, Australia
[b] Centre for Technology in Water and Wastewater, School of Civil and Environmental Engineering, Faculty of Engineering and Information Technology, University of Technology Sydney, 15 Broadway, NSW 2007, Australia
[c] Department of Environmental Science and Disaster Management, Noakhali Science and Technology University, Noakhali 3814, Bangladesh
[d] Department of Materials Engineering and Convergence Technology, Gyeongsang National University, Jinju 52828, Republic of Korea

HIGHLIGHTS

- Novel integrated brine electrolyzer for the circularity of green hydrogen, oxygen, and resources
- PVA-TEAOH-KOH-30 wt% SWE delivers an excellent current density of 375 mA cm^{-2}.
- The 9× concentrated brine, achieved through a volume concentration factor (VCF), could be a potential source of resources for diverse applications.
- Overcome electrode corrosion, unwanted side reactions, and gas cross-over issues

GRAPHICAL ABSTRACT

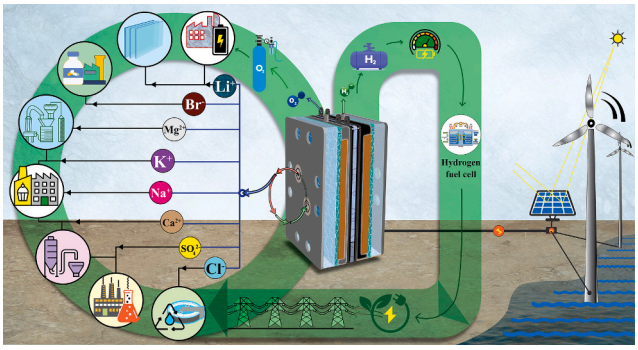

ARTICLE INFO

Keywords:
Renewable energy
Impure water
Self-wetted electrolyte
Breathable oxygen
Tetraethylammonium hydroxide
Resources
Brine

ABSTRACT

This paper investigates the circularity of green hydrogen and resource recovery from brine using an integrated approach based on alkaline water electrolysis (AWE). Traditional AWE employs highly alkaline electrolytes, which can lead to electrode corrosion, undesirable side reactions, and gas cross-over issues. Conversely, indirect brine electrolysis requires pre-treatment steps, which negatively impact both techno-economics and environmental sustainability. In response, this study proposes an innovative brine electrolysis process utilizing solid electrolytes (SELs). The process includes an on-site brine treatment facility leveraging a self-driven phase transition technique and incorporates a hydrophobic membrane as part of a membrane distillation (MD) system to facilitate the gas pathway. Polyvinyl alcohol (PVA) and tetraethylammonium hydroxide (TEAOH)-based electrolytes, combined with potassium hydroxide (KOH) at various concentrations, function as a self-wetted

* Corresponding author.
** Correspondence to: H.K. Shon, ARC Research Hub for Nutrients in a Circular Economy, School of Civil and Environmental Engineering, Faculty of Engineering and Information Technology, University of Technology Sydney, 15 Broadway, NSW 2007, Australia.
E-mail addresses: walden@gnu.ac.kr (S.Y. Nam), Hokyong.Shon-1@uts.edu.au (H.K. Shon).

https://doi.org/10.1016/j.desal.2025.118580
Received 4 December 2024; Received in revised form 14 January 2025; Accepted 14 January 2025
Available online 15 January 2025

electrolyte (SWE). This design partially disperses water vapor while effectively preventing the intrusion of contaminated ions into the SWE and electrode-catalyst interfaces. PVA-TEAOH-KOH-30 wt% SWE demonstrated the highest ion conductivity (112.4 $mScm^{-1}$) and excellent performance with a current density of 375 mA cm^{-2}. Long-term electrolysis confirmed with a nine-fold brine in volume concentration factor (VCF) demonstrated stable performance without MD membrane wetting. The Cl^-/ClO^- and Br^- concentrations in the SWE were reduced by five orders of magnitude compared to the original brine. This electrolyzer supports the circular use of resources, with hydrogen as an energy carrier and concentrated brine and oxygen as valuable by-products, aligning with the sustainable development goals (SDGs) and net-zero emissions by 2050.

1. Introduction

Energy, a quantifiable entity that can be transformed into various forms, is fundamental to human progress. As the global population grows and technology continues to advance, the demand for energy has escalated into a critical concern [1,2]. The challenge of identifying sustainable and efficient energy sources has become one of the most pressing issues of the 21st century. Achieving sustainability and decarbonizing the energy sector is vital to meeting the sustainable development goals (SDGs) and reaching net-zero emissions by 2050. A key solution lies in shifting from traditional, fossil-fuel-based greenhouse gas (GHG)-intensive energy sources to a future powered by green renewable energy [3].

Researchers today are actively seeking alternative energy sources to reduce the carbon footprint and ensure sustainable global energy security. Green hydrogen, a highly promising energy carrier, stands out as one of the most viable renewable energy sources for decarbonizing the global energy landscape. Its transformative properties, such as high calorific value, the highest energy content per unit mass and exceptional thermal stability with the highest energy density, make it particularly appealing [1,4]. Most importantly, green hydrogen does not emit GHGs during system operation, making it a key component for integration into the current renewable energy domain to meet SDGs and net-zero emissions targets. However, the current energy system operates under a linear economic (LE) model of take-make-use-dispose, which makes it vulnerable and less economically viable. For example, traditional fossil fuel-based energy systems rely on the continuous extraction of finite natural resources, leading to resource depletion and increased costs over time without considering the recycling or reuse of the resources or energy [3]. Incorporating a circular economy (CRE) approach into green energy production technologies has the potential to reduce energy production costs while recovering valuable resources from the water industry (WI). This transition could ensure the circular use of hydrogen, breathable oxygen, and other resources, further supporting the SDGs [1,5].

Classical green hydrogen production technologies are generally categorized into three main types based on the energy sources they require: proton exchange membrane water electrolysis (PEMWE), alkaline water electrolysis (AWE), and anion exchange membrane water electrolysis (AEMWE) [6]. While PEMWE and AWE are well-developed and widely commercialized across various countries, AEMWE remains less mature. However, all of these technologies, with the exception of AEMWE, require ultra-pure water to produce high-purity hydrogen (99.99 %) during operational processes [7]. It is estimated that producing 1 kg of green hydrogen via water electrolysis requires 11 L of deionized (DI) water. Yet, the actual volume of high-quality raw water needed to generate the same amount of hydrogen ranges from 60 to 95 L [8]. As such, ensuring a sustainable hydrogen economy (HE) may face a significant challenges in securing an adequate supply of fresh, pure water [9]. Impure water sources, including wastewater, seawater and brine, could serve as viable alternatives for water electrolysis and hydrogen production [6,10,11]. These alternative water sources also present an opportunity to recover valuable resources, such as metals, minerals, and nutrients.

Few studies have investigated the potential of direct seawater electrolysis for hydrogen production [12–14]. In contrast, several studies have examined integrated approaches that combine preliminary filtration of seawater or wastewater with water electrolysis, producing purified water for hydrogen generation [15]. For instance, reverse osmosis (RO), ultrafiltration (UF), and forward osmosis (FO)-coupled indirect or integrated seawater electrolysis methods have been extensively investigated [16–18]. Although these pretreatment processes effectively block ions and impurities, directing treated water into the electrolyte solution, the membranes used in these technologies lack complete selectivity and cannot fully inhibit chlorine chemistry or prevent electrode corrosion. However, the use of highly alkaline electrolytes in AWE and AEMWE systems during impure water electrolysis presents various challenges. In these conditions, chloride ions (Cl^-) undergo oxidation, which competes with the oxygen evolution reaction (OER) and leads to the formation of corrosive and toxic by-products, such as hypochlorite (ClO^-) and chlorine gas (Cl_2). Besides, the corrosion issue of electrodes was not only limited to chlorine chemistry but also caused by halides, especially bromide (Br^-) and other ions [16,18,19]. The presence of these species not only creates a hazardous environment but also compromises the production of pure, breathable oxygen, simultaneously reducing the overall cell performance and increasing the hydrogen production costs [16,20–22]. Considering the challenges raised in recent direct, indirect, and integrated impure water/seawater electrolysis methods, there is a critical need for innovative approaches that can mitigate issues such as ion intrusion, electrode corrosion, and the formation of undesirable by-products while enhancing system efficiency and sustainability.

This paper examines the circularity of green hydrogen production and resource recovery from brine through an innovative and integrated approach rooted in AWE principles. The conventional AWE process relies on the use of a highly alkaline liquid electrolyte to enhance ion conduction in the feed solution. However, this method leads to several challenges, including electrode corrosion and undesirable side reactions, particularly when dealing with the complex composition of brine or other impure water sources [11]. While advanced catalysts have mitigated corrosion to some extent [10,11], indirect brine electrolysis, which requires pre-treatment, introduces additional maintenance requirements and energy consumption. This ultimately renders brine electrolysis inefficient from both techno-economic and environmental perspectives.

In this study, the brine electrolysis system integrates an on-site brine treatment process utilizing a self-driven phase transition technique. A hydrophobic membrane is employed, functioning as part of a membrane distillation (MD) process that supports the gas pathway interface, making it both water-resistant and breathable. Furthermore, an array of potassium hydroxide (KOH)-based solid electrolytes (SELs), incorporating tetraethylammonium hydroxide (TEAOH), was introduced to act as a self-wetted electrolyte (SWE), replacing the need for highly concentrated alkaline liquid electrolytes. TEAOH is a quaternary ammonium salt that dissociates into tetraethylammonium (TEA^+) and hydroxide (OH^-) ions, both of which are relatively mobile and can enhance ion transport within the solid ELs. The presence of these ions introduces additional charge carriers, which contributes directly to an increase in ion conductivity [10,11]. Moreover, TEAOH is highly hygroscopic, meaning it attracts and retains water molecules even in solid

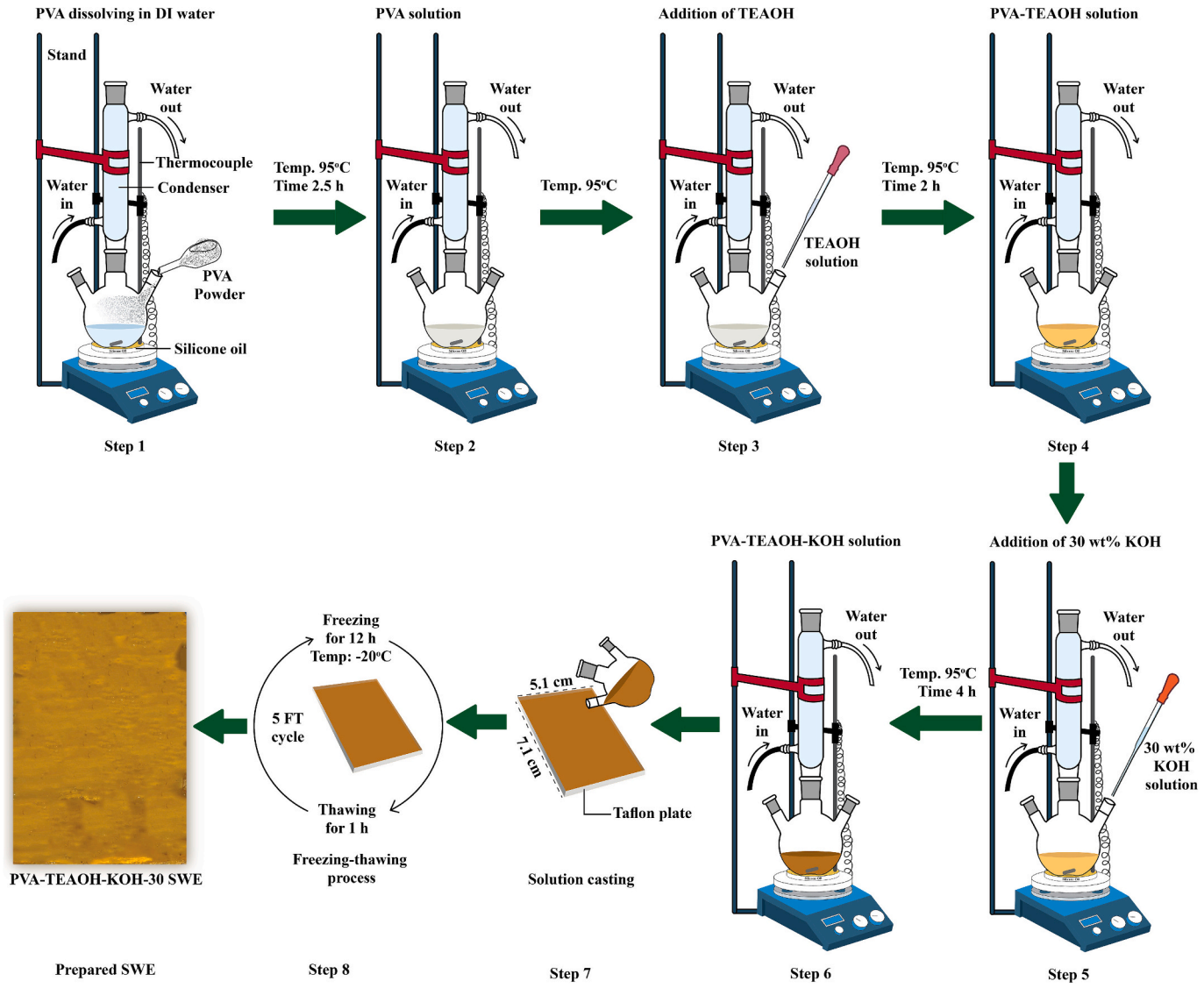

Fig. 1. Synthesis procedures of self-wetted electrolytes (SWEs) by freezing-thawing techniques.

or semi-solid materials. When incorporated into a SEL, TEAOH facilitates water absorption and retention within the electrolyte structure. This retained water can serve as a medium for ion transport, as ions move more readily in hydrated environments than in dry, solid matrices [11,23,24].

This design allows for the partial dispersion of water vapor while fully preventing the intrusion of brine and contaminated ions into the system. During system operation, continuous brine evaporation on the brine side and water vapor dispersion within the membrane on the SWE side is driven by the variation in vapor pressure between the brine and the SWE, mediated by the MD membrane. Inside the membrane, the water vapor condenses into liquid form through contact with the SWEs. This phase-changing mechanism allows for the production of pure water from the brine while ensuring complete ion retention in the brine chamber. Simultaneously, the produced pure water undergoes electrolysis via the SWE, with the process sustained by the pressure difference at the interface. Once equilibrium is reached, where the rate of water transportation matches the rate of electrolysis, a continuous and steady flow of water is established through a "liquid-gas-liquid" transport mechanism. This ensures a reliable supply of fresh water for electrolysis while fully retaining ions from the brine source.

In essence, the primary goal of this investigation is to develop a circular economy (CRE)-based, sustainable energy-generating process that offers a viable solution to future energy challenges. This process is aimed at supporting the development of a future hydrogen economy (HE), an oxygen economy (OE), and sustainable resource management by closing the resource loop. The system holds significant potential for areas where continuous electricity supply is limited, and there is a severe scarcity of non-frozen freshwaters, such as desert regions, remote islands, and densely populated urban centers worldwide.

2. Experimental

2.1. Materials and chemicals

Polyvinyl alcohol (PVA) (MW: 195,000), potassium hydroxide (KOH), tetraethylammonium hydroxide (TEAOH, 35 wt%), sodium chloride (NaCl), potassium sulfate (K_2SO_4), lithium chloride (LiCl), magnesium sulfate ($MgSO_4$), isopropyl alcohol (IPA), calcium chloride ($CaCl_2$) and potassium bromide (KBr) were purchased from Sigma Aldrich, Korea. The MD membrane, consisting of polytetrafluoroethylene (PTFE) having a pore size of 0.2 μm and a thickness of 200 μm, was bought from Sterlitech Corporation, USA. The melamine foam was purchased from Daiso, Australia. The ZIRFON gas separator was acquired from AGFA, Belgium. The components of catalysts, i.e., platinum on carbon (Pt/C) and IrO_2, were obtained from Tanaka, Japan and Alfa

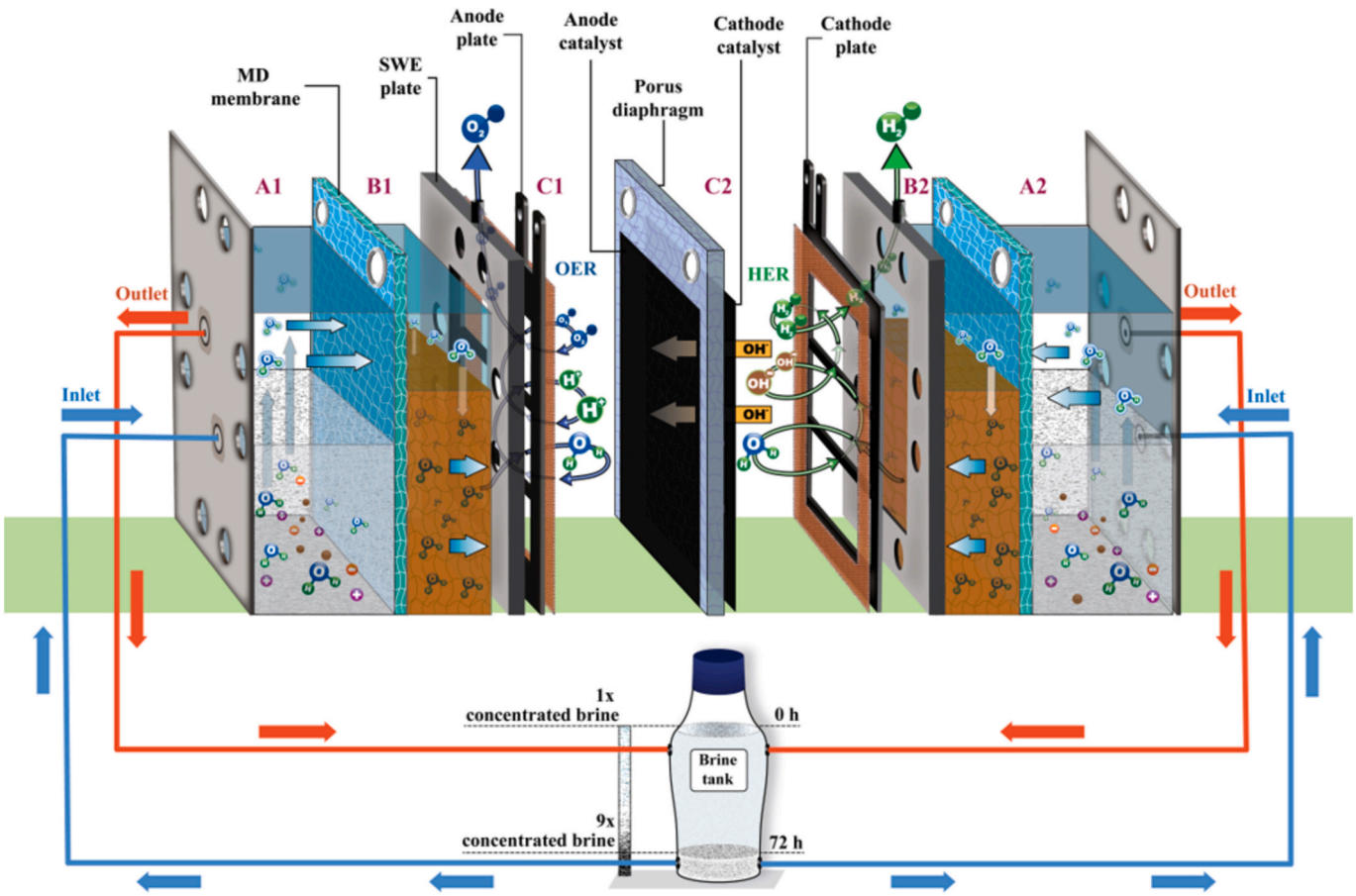

Fig. 2. Schematic illustration of the brine electrolysis process. On-site brine treatment has been conducted with the aid of membrane distillation and self-wetted electrolytes to produce pure water for electrolysis. A1 and A2 indicate the brine chambers; these are the entry points of brine into the electrolyzer. The brine undergoes continuous recirculation through these chambers into the brine tank. B1 and B2 illustrate the SWE chambers, whereas C1 and C2 represent the anode electrode-catalyst interface and cathode electrode-catalyst interface, respectively. The water vapor passed through the MD membrane in the SWE chamber, where it re-liquefied due to the vapor pressure difference between the brine and SWE.

Aeser, USA, respectively. The ionomer solution and gas diffusion layer (GDL) were sourced from Fumatech, Germany, and CNL Energy, Korea, respectively. The synthetic brine was prepared by dissolving a homogeneous mixture of salts in deionized (DI) water to achieve the following ion concentrations: Li^+ (0.1 g/L), Na^+ (33.5 g/L), K^+ (1.9 g/L), Mg^{2+} (0.4 g/L) and Ca^{2+} (5.02 g/L).

2.2. Synthesis and characterization of PVA-KOH-based solid electrolytes (SELs) incorporating TEAOH

The PVA-KOH-based ELs were synthesized following the freeze-thaw (FT) techniques [25]. A 3 wt% PVA was dissolved in 9 mL of DI water in a three-necked flask and stirred magnetically for 2.5 h in a closed reflux system at 95 °C. The resulting solution was then mixed with 18 mL of TEAOH and stirred under the same conditions for an additional 2 h. Subsequently, varying concentrations of KOH solution (20–40 wt%) were added to the mixture, which was continuously stirred for another 4 h while maintaining the same experimental parameters. The prepared EL was then cast onto a Teflon plate and stored at −20 °C for 12 h to expedite the cross-linking process. The FT cycle was repeated five times to complete the EL formation where freezing and thawing time were 12 and 1 h, respectively. PVA-KOH ELs were synthesized using the same method, ensuring consistent PVA content and OH^- ion concentration. To synthesize the melamine-supported PVA-KOH and PVA-TEAOH-KOH ELs, different wt% (KOH) of the prepared ELs were immersed in the melamine foam (7.1 cm × 5.1 cm) for 1 h, followed by the FT cycles for cross-linking, as previously described. The PVA-based ELs with a Y% KOH solution were denoted as PVA-KOH Y% and PVA-TEAOH-KOH Y%, where Y refers to the wt% of the KOH solution. When integrated with melamine foam, these were labeled as melamine (M)-PVA-KOH Y% and M-PVA-TEAOH-KOH Y%. The schematic of the SWEs preparation has been provided in Fig. 1. The synthesized ELs were characterized in terms of morphology, as well as electrochemical and dimensional stability. Detailed characterization procedures are provided in supplementary information S1.

2.3. Fabrication of membrane-electrode assembly (MEA)

The membrane electrode assembly (MEA) was fabricated using gas diffusion electrode (GDE) techniques [26]. In brief, the catalyst ink for the anode was prepared by mixing 29.59 mg of IrO_2 powder, 126 mg of binder/ionomer solution, and 5 g of isopropanol (IPA) in a glass vial. A separate vial was also prepared containing 10.87 mg of Pt/C powder, 46.5 mg of binder/ionomer solution, and 5 g of IPA for the cathode ink. Both mixtures were vortexed for 5 min, followed by 2 h of ultrasonication. The prepared catalyst inks were then carefully sprayed onto the gas diffusion layer (GDL) homogenously using an air-gun sprayer (GP-2, CNL, Korea). The anode was coated with 2.0 mg cm^{-2} of IrO_2, while the cathode was coated with 0.4 mg cm^{-2} of Pt/C.

2.4. Brine electrolysis system

The brine electrolysis system incorporates an on-site brine treatment process, utilizing a self-driven phase transition technique. We employed

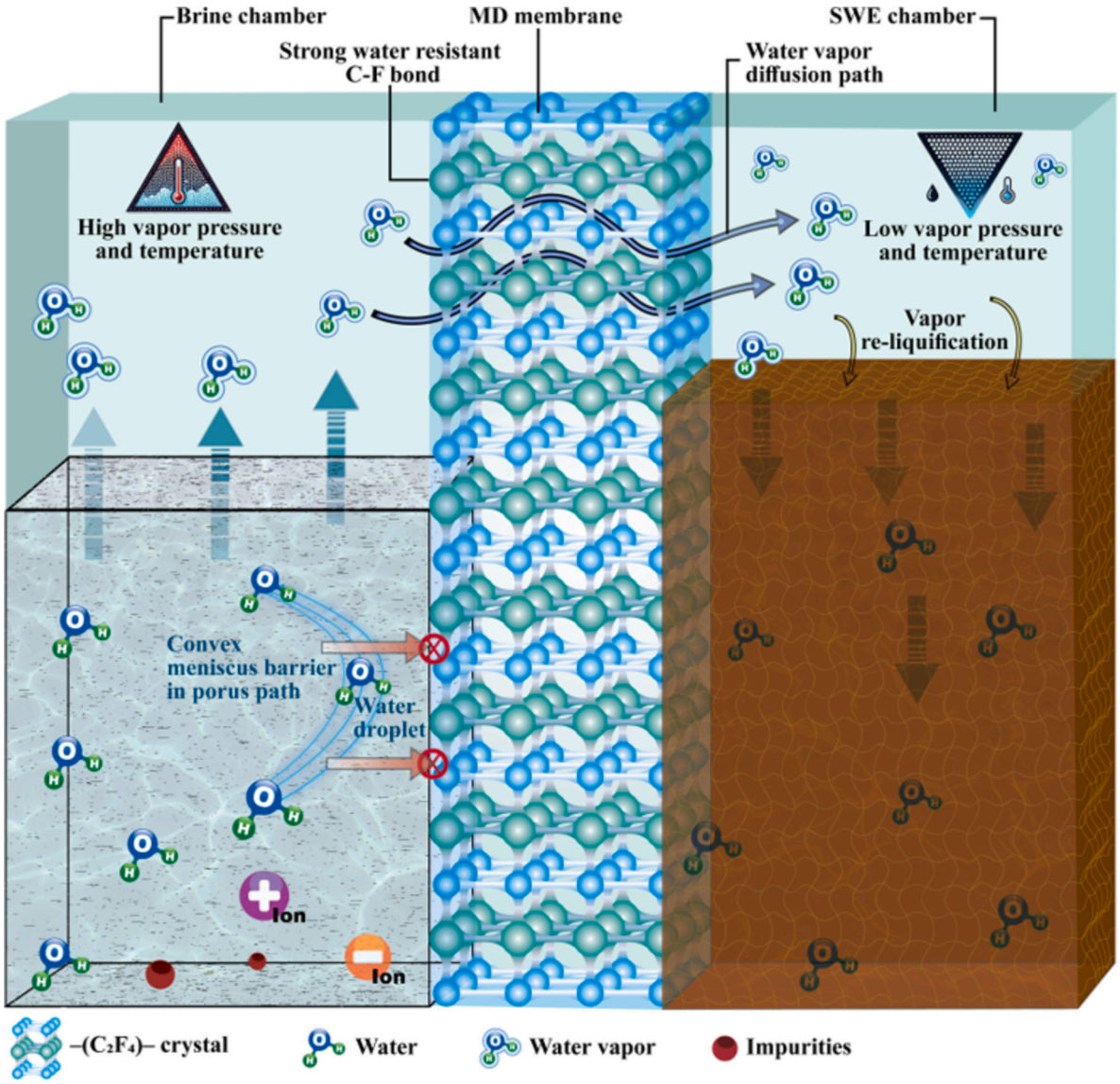

Fig. 3. Illustration of on-site brine treatment mechanisms by MD membrane and PVA-TEAOH-KOH-based self-wetted electrolytes. The water molecules remain in a liquid state in the brine chamber, then convert into a gaseous state while transporting through the MD membrane and re-liquefies upon reaching the SWE chamber.

a hydrophobic membrane, to facilitate the water vapor pathway, which is both water-resistant and breathable. Additionally, an array of PVA-KOH-based solid ELs was incorporated into the rectangular space of the SWE plate to function as a self-wetted electrolyte (SWE) (Fig. 2). This design facilitates the partial dispersion of water vapor while completely preventing the intrusion of brine and contaminated ions. During the system operation, the dynamic force for continuous brine evaporation on the brine side and dispersion of water vapor within the membrane on the SWE side is achieved by the variation in the vapor pressure of water between the brine and SWE, mediated by the MD membrane. The vapor inside the membrane is re-liquified by the SWEs. This phase-changing mechanism enables the production of pure water from the brine source with 100 % ion-retention efficiency. Simultaneously, the produced water undergoes concurrent electrolysis facilitated by the SWE, maintaining the interface vapor pressure difference. A convex meniscus is formed in the pores of the MD membrane when water comes into contact with the surface (Fig. 3). This is due to the high surface tension of water and the non-polar nature of the hydrophobic membrane material. Upon reaching equilibrium, where the water transportation rate matches the electrolysis rate, a mode of continuous and constant water transport is established through the "liquid-gas-liquid" mechanisms. The SWEs underwent distinct stages of swelling i.e., dry crystals (prior to operation) and a mixture of crystals and saturated solution (during operation) which is essential for keeping the steady-state shape and volume of SWEs. The simultaneous transport and electrolysis of water ensured that the volume remained nearly constant, allowing the SWE to remain confined within the frame of the SWE plate. This process reliably delivers fresh water for electrolysis while ensuring complete ion retaining from the brine source.

2.5. Cell performance and durability analysis

The cell performance was evaluated using two feed sources, i.e., DI water and brine, for comparative analysis. The feed temperature was maintained at 35 °C using a temperature controller, and the flow rate was set at 210 mL min^{-1}. The feed solution was re-circulated into the brine chamber (Fig. 2). The effective cell area was 25 cm^2, while the MD membrane had an effective surface area of 6.7 cm^2. Current-voltage (C—V) measurements were conducted using a DC power supply (MK6005P, Korea), with the voltage gradually increased from 1.4 to 4.0 V. Durability testing was carried out with an impedance analyzer (ZIVE MP5, WonA Tech, Korea) under a constant current of 375 mA cm^{-2} over

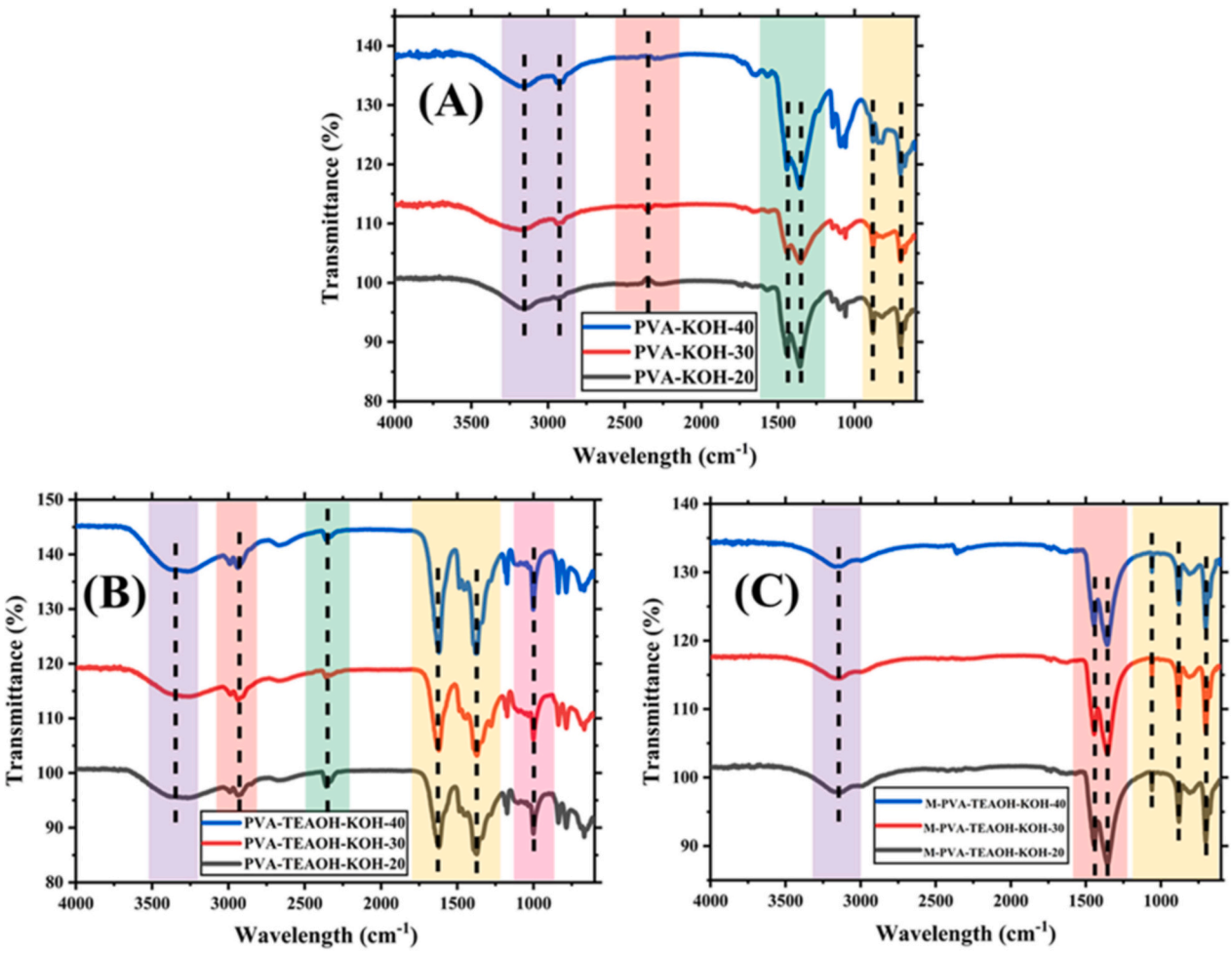

Fig. 4. FTIR spectra of self-wetted electrolytes: (A) PVA-KOH, (B) PVA-TEAOH-KOH, and (C) M-PVA-TEAOH-KOH.

a 72-h period to assess lab-scale, long-term brine electrolysis performance. The concentrations of produced hydrogen and oxygen were measured using a Gilibrator pump (Sensidyne, USA). Brine concentration was monitored over the 72-h durability test at 24-h intervals to evaluate potential resource recovery options. Linear sweep voltammetry (LSV) was performed using a multimeter, and the corresponding anode and cathode voltages were recorded at varying current densities of 0, 50, 100, 150, 200, 250, 300, 350, and 400 mA cm^{-2}.

2.6. Determination of ion concentrations and MD membrane wetting

The concentrations of cations (Li^+, Na^+, K^+, Ca^{2+}, and Mg^{2+}) and anions (Cl^-, Br^-, and SO_4^{2-}) in the brine and SWE were determined using ion chromatography (Dionex DX-3000, USA) with IonPac CS17 and IonPac AS11-HC analytical columns, respectively, at every 24 h intervals up to 72 h of brine electrolysis. The concentration of hypochlorite (ClO^-) in SWE was measured using the *o*-tolidine method [21]. Specifically, 0.5 mmol of *o*-tolidine was dissolved in DI water to prepare the testing solution. Various concentrations of ClO^- (0, 2, 4, 8, 16, 32, and 65 μM) were added to 1.5 mL of KOH solution and mixed with the *o*-tolidine solution. A standard calibration curve was then generated by measuring the optical density (OD) at a wavelength of 436 nm. After long-term brine electrolysis, a portion of the SWE was added to the testing solution, and the concentration of ClO^- was determined by comparing the results to the standard calibration curve [17]. The MD membrane fouling was characterized by morphology, elemental composition and surface functional group analysis using FESEM-EDX (JEOL, Model: JSM-7610F, Germany), FTIR and contact angle measurement techniques.

3. Results and discussion

3.1. Characterization of self-wetted electrolytes

3.1.1. Morphology and chemical functionalities

To verify the morphology, chemical structure, and anticipated characteristics of the synthesized SWEs, we employed Fourier Transform Infrared Spectroscopy (FTIR), Field Emission Scanning Electron Microscopy (FESEM), and Energy Dispersive X-ray Spectroscopy (EDX) analysis. The FTIR spectrum confirmed the expected surface functionalities and chemical compositions of the SWEs. Distinct characteristic peaks were observed in the SWE, aligning with their intended chemical structures, as illustrated in Fig. 4. All three SWEs displayed strong, broad O—H stretching peaks, indicative of hydroxyl groups, within the wavelength range of 3322–3167 cm^{-1}. The PVA-TEAOH-KOH and PVA-KOH SWEs exhibited carbonyl (C=O) stretching at 2359 cm^{-1} and 2360 cm^{-1}, respectively. In contrast, the M-PVA-KOH-TEAOH showed a carboxylic acid (-COOH) stretching peak at 1737 cm^{-1}.

Additionally, the C—H stretching and bending peaks were detected in PVA-KOH and M-PVA-KOH-TEAOH at 2840 and 1445 cm^{-1}, individually, indicating the presence of alkane groups that were absent in PVA-TEAOH-KOH SWE. Furthermore, the characteristic -NH_2 group was identified in PVA-TEAOH-KOH and M-PVA-KOH-TEAOH at 1629 cm^{-1} and 1060 cm^{-1}, correspondingly confirming the incorporation of TEAOH and melamine into the SWE matrix [18,27]. These results provide valuable insights into the chemical functionalities and structural

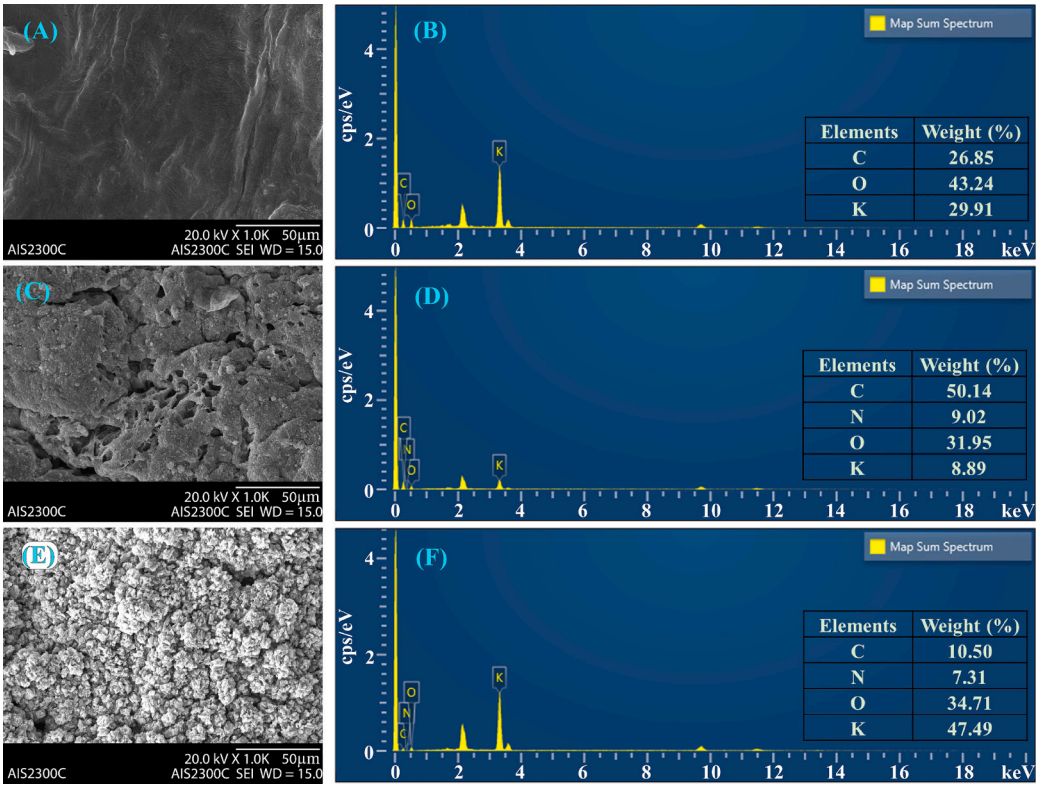

Fig. 5. FESEM micrographs and EDX analysis results of self-wetted electrolytes. (A, B) PVA-KOH-30, (C, D) PVA-TEAOH-KOH-30 and (D, E) M-PVA-TEAOH-KOH-30.

integrity of the synthesized SWEs, highlighting their potential applications. Additionally, the C═C bending peak at 701 cm^{-1} is distinctive to M-PVA-KOH-TEAOH, as its presence clearly indicates the incorporation of melamine in this SWE [28]. Among all the SWEs, PVA-TEAOH-KOH demonstrates robust hydrogen bonding and features the -NH_2 group due to the addition of TEAOH, which significantly enhances the reactivity and stability of this SWE.

FESEM micrographs and EDX analysis results of the SWEs are presented in Fig. 5. The PVA-KOH-based SWE showed compact, homogeneous and dense-like properties (Fig. 5A) [27]. In contrast, the PVA-TEAOH-KOH (Fig. 5C) SWE illustrates a highly porous structure with visible pores and an irregular surface topology. These features can be attributed to the addition of TEAOH in the SWE's matrix because TEAOH is a quaternary ammonium salt, which could increase the porosity of the PVA-TEAOH-KOH SWE [23]. Although melamine incorporation enhances the structural strength of SWE, it showed a densely packed surface area with granular foam structures and thinner pores formation compared to PVA-TEAOH-KOH SWE (Fig. 5E). The irregular and discernible bright spots in the SWE's matrix indicated the precipitation of KOH particles [11]. FESEM micrographs of SWEs with different KOH concentrations are provided in Fig. S1 and their corresponding discussion has been added in the supplementary information 2.

The EDX analysis of the SWEs revealed distinct elemental compositions that underscore their unique chemical structures (Fig. 5B, D and F). The EDX spectrum of PVA-KOH SWE showed 26.85, 43.24 and 29.91 % of carbon (C), oxygen (O) and potassium (K), respectively, indicating the presence of hydroxyl groups and K whereas in the case of PVA-TEAOH-KOH SWE, the supplementation of TEAOH is evident from the increased contents of C and O, and the presence of 9.02 % nitrogen in the SWE's matrix [29]. This composition suggests enhanced hydrogen bonding and water retention capabilities. The M-PVA-KOH-TEAOH spectrum showed a higher K content (47.49 %) and a notable presence of nitrogen (7.31 %), reflecting the contributions of both TEAOH and melamine, which enhance the material's structural integrity and reactivity.

3.1.2. *Dimensional and electrochemical stability*

The ion conductivity data of the synthesized SWEs is illustrated in Fig. 6A. According to the electrochemical standpoint, high ion conduction through the SWEs could serve efficient ion transport between electrodes, enhance catalytic performance, and subsequently increase the hydrogen evolutionary reaction (HER) and oxygen evolutionary reaction (OER) reactions by minimizing energy losses, reducing overpotentials, and improving the overall efficiency of electrochemical reactions involved in water splitting [30–32]. However, PVA-KOH-20, PVA-TEAOH-KOH-20 and M-PVA-TEAOH-KOH-20 SWEs provided the highest ion conductivity of 169, 142 and 99 mS cm^{-1}, respectively. In contrast, the lowest ion conductivity was recorded in PVA-KOH-40, PVA-TEAOH-KOH-40 and M-PVA-TEAOH-KOH-40 wt% SWEs.

It was noted that increasing wt% of KOH decreased the ion conductivity of SWEs. The increased KOH content increases the crosslinking density of SWEs, which results in increased viscosity and decreased swelling ratio, affecting the amount of water available for ion transport and increased ion pairing and precipitation [28]. Moreover, high KOH concentrations can lead to the presence of other competing ions, which can disrupt the balance and mobility of the primary conducting ions. These issues increased the ohmic resistance of the SWEs and provided minimum ion conduction at elevated KOH concentrations [6]. However, only PVA-TEAOH-KOH SWE showed stable ion conductivity over a wide range (20–40 wt%) of KOH treatments. The exceptional capabilities of this SWE could be the addition of TEAOH to the polymer matrix because TEAOH is a quaternary ammonium compound that can increase ion conductivity and have high water retention capacity (WRC) (Fig. 6B) [33]. The PVA-TEAOH-KOH SWE can retain 50 % of water after 24 h, whereas the PVA-KOH and M-PVA-TEAOH-KOH SWEs can retain only 5 and 20 % of water, correspondingly (Fig. 6B). The SWR and WU varied with temperature (Fig. 5C). The highest WU and SWR were observed at 40 °C. These results indicated that the shrinkage nature of the previous SWE is much less compared to the later SWEs, which is considered highly significant in solid electrolyte-based electrolysis of impure water

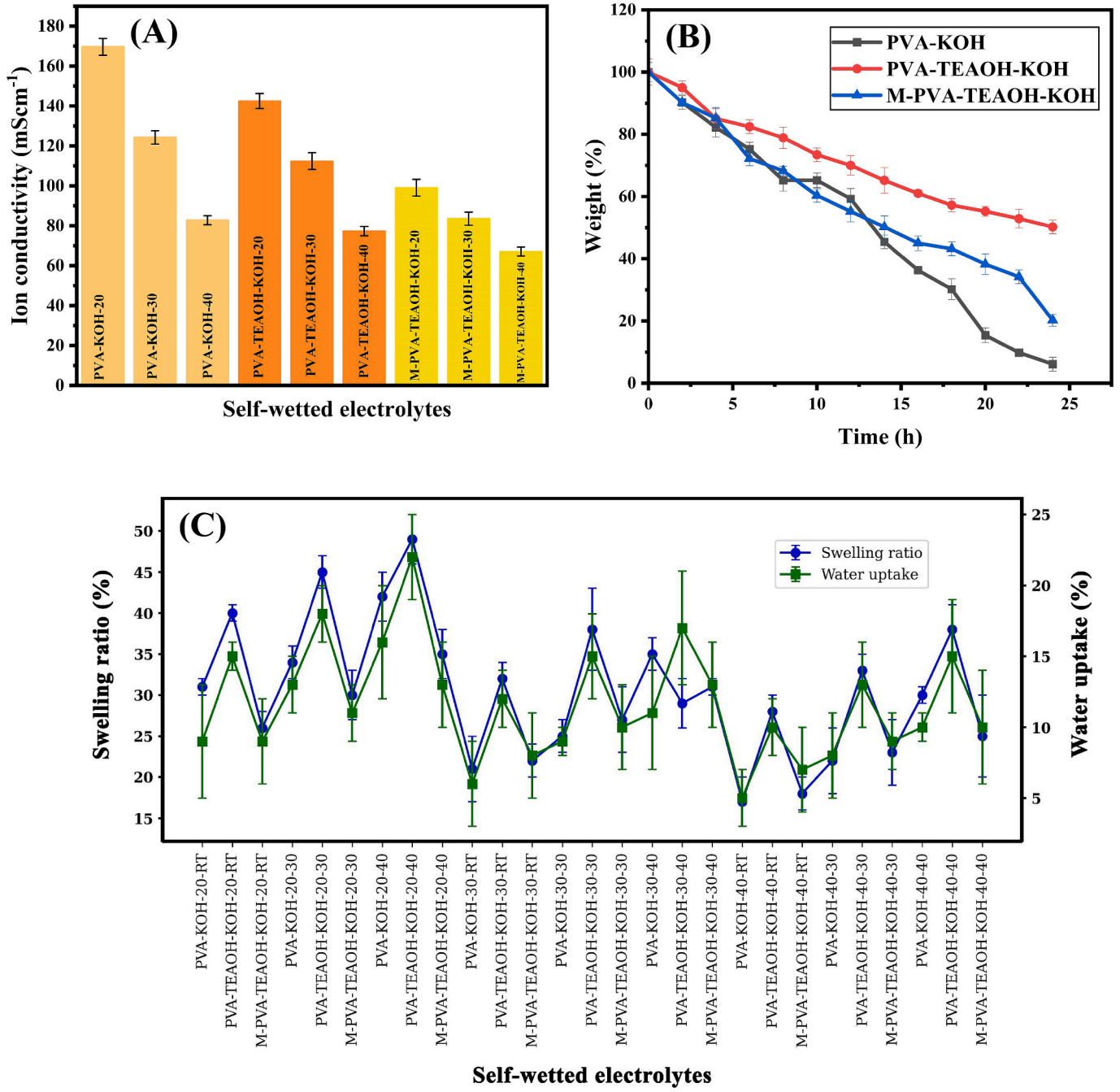

Fig. 6. (A) Variations of ion conductivity in different SWEs, (B) water retention (%) capacity of SWEs at different times (h). and (C) SWR and WU of SWEs in various temperatures (25 to 40 °C). RT indicates room temperature.

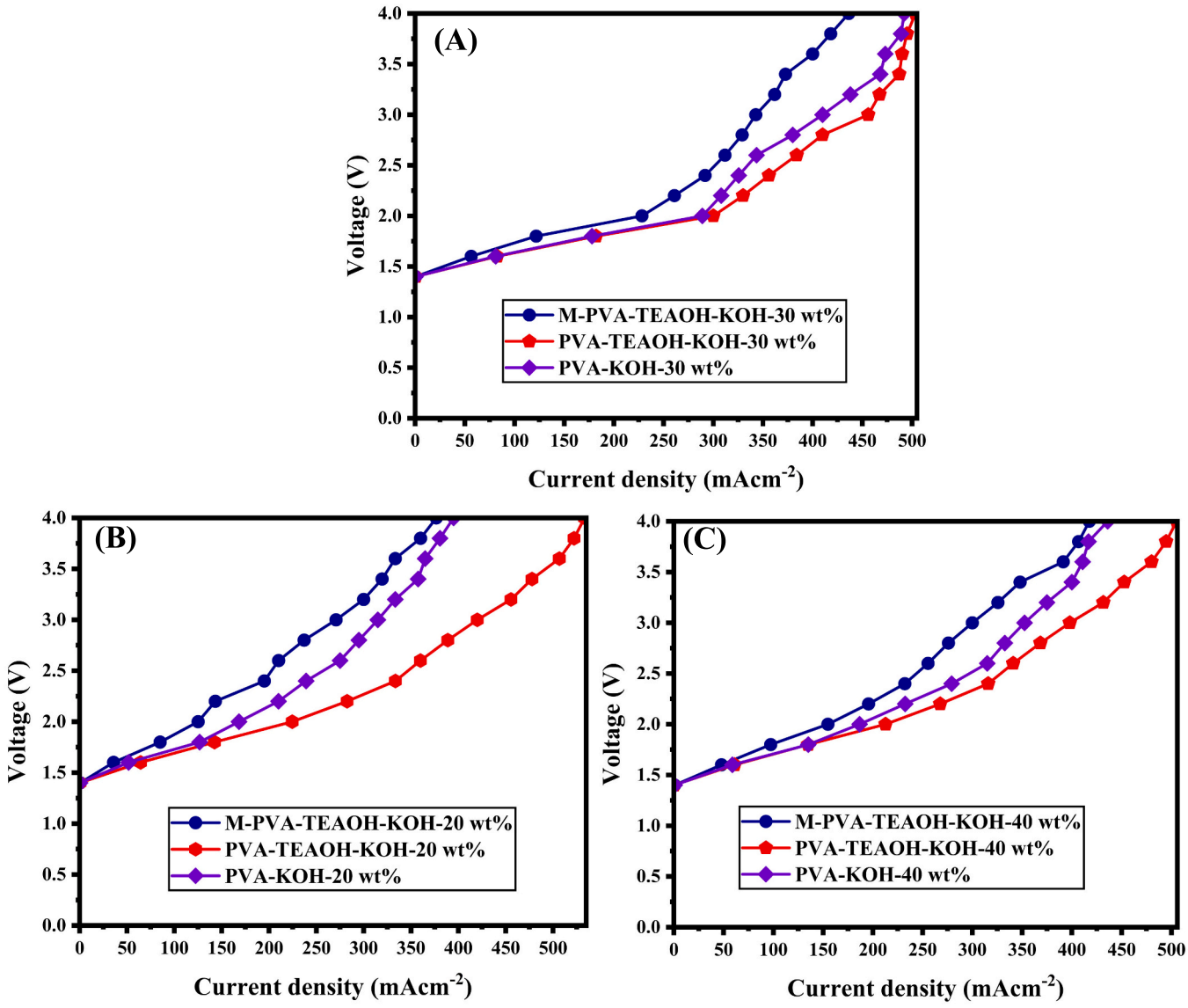

Fig. 7. I-V curve of single-cell performance of DI water feed having various SWEs: (A) Variations of current densities with respect to varying voltages for 30 wt% KOH containing SWEs, (B) 20 wt% KOH containing SWEs and (C) 40 wt% KOH containing SWEs.

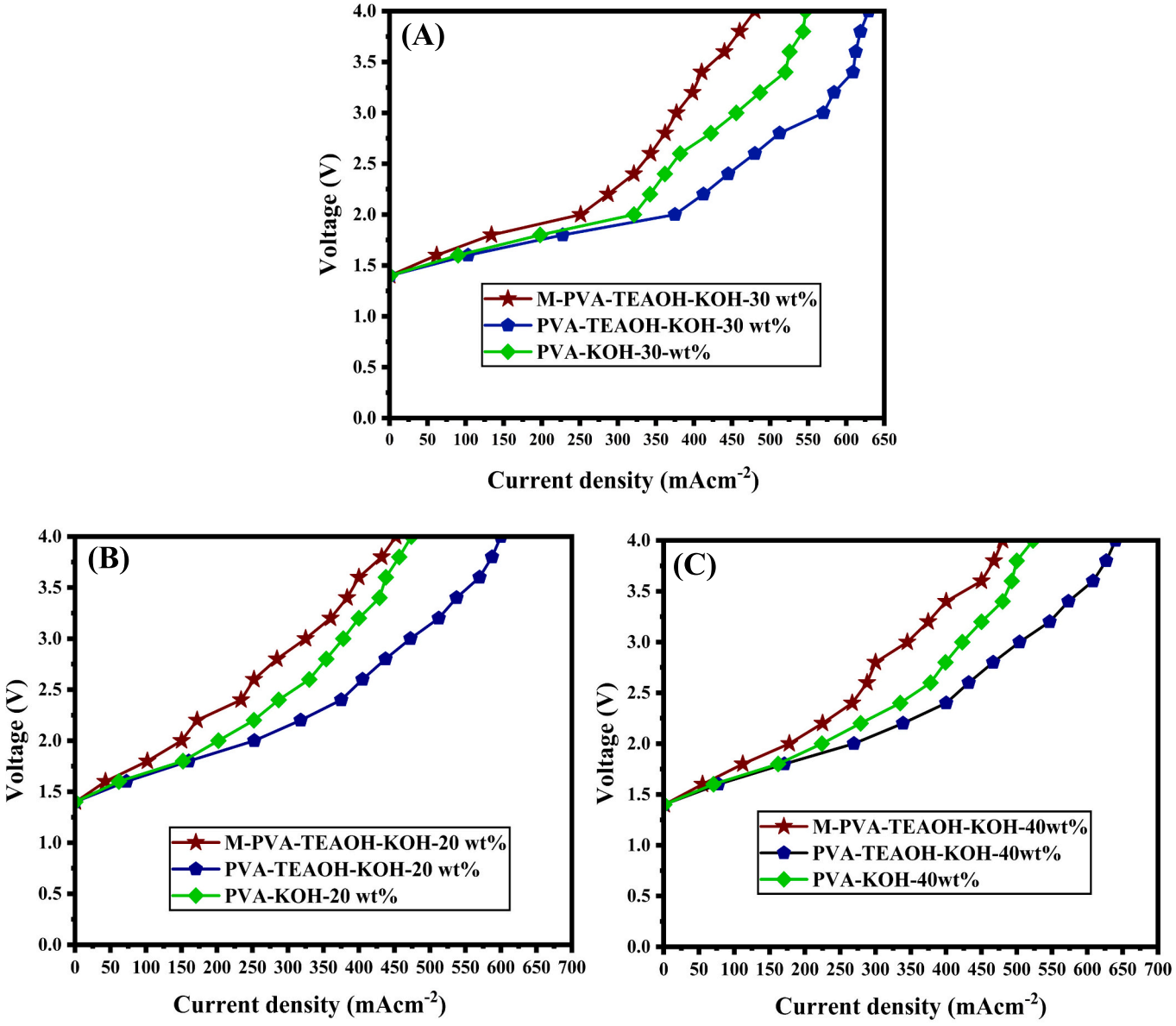

Fig. 8. I-V curve of single-cell performance of brine having various SWEs; (A) variations of current densities with respect to varying voltages for 30 wt% KOH containing SWEs, (B) 20 wt% KOH containing SWEs and (C) 40 wt% KOH containing SWE.

Table 1
Comparison of cell performances with the existing literature and the present study.

SL. no.	Electrolyte composition	Feed solution	Pre-treatment requirement	Catalysts used	Highest current density (mA cm^{-2})	Operating voltage (V)	Operating temperature (°C)	Ref.
1	PVA-TEAOH-KOH-30 wt%	Synthetic brine	None	IrO_2, Pt/C	375	2	35	[This study]
2	PVA-KOH 30 wt%	Urine	MBR[b]	IrO_2, Pt/C	204.35	2	35	[6]
3	PVA-KOH 40 wt%	Natural seawater	None	MoNi/NF	250	1.95	25–30	[16]
4	1.0 M KOH + 0.5 M NaCl + 0.5 M urea	Synthetic seawater	None	NiFeSP	500	1.94	30	[39]
5	1.0 M KOH + 0.5 M NaCl + 0.1 M N_2H_4	Synthetic seawater	None	Co-Ni-P/CP	500	0.533	35	[40]
6	1.0 M KOH + seawater + 0.5 M methanol	Natural seawater	RO[a]	$NiFe_2O_4$/NF	100	1.74	25	[37]
7	Seawater + 0.7 M $[Fe(CN)_6]^{4-}$	Natural seawater	RO[a]	Prussian blue	320	1.7	30	[41]
8	1.0 M KOH + seawater + 0.1 M xylose	Natural seawater	None	NiCoP	100	1.57	25	[42]
9	1.0 M KOH + 0.171 M NaCl + 1 M H_2SO_4	Synthetic brine	None	NiFe-LDH	100	2.1	25	[43]
10	0.6 M Na_3PO_4 + 0.1 M NaOH	Synthetic seawater	Integrated FO[c]	NiFe-Ar-P	360	2.10–2.15	25	[19]
11	Municipal wastewater + 1.0 M KOH	Natural seawater	Integrated FO[c]	Ni	400	2	25–40	[44]
12	0.6 M NaCl + 3 M KCl + 50 % HNO_3	Synthetic seawater	Integrated FO[c]	Pt-Ag/AgCl	250	2.80	25	[45]
13	Wastewater + 93 % NaOH + 5 M KOH	Synthetic and raw wastewater, effluent and surface water	UF[d]	Ni	60.14–45.82	9	24–26	[46]

[a] RO = reverse osmosis.
[b] MBR = membrane bioreactor.
[c] FO = forward osmosis.
[d] UF = ultra filtration.

for hydrogen generation [34].

However, it should be noted that the WU and SWR of PVA-TEAOH-KOH were highest compared to other SWEs (Fig. 6C). The supplementation of TEAOH in the PVA could lead to increased water retention ability, as evident by the water retention experiment's results described above. On the other hand, melamine foam had a densely packed rigid structure. Thus, the addition of TEAOH did not help to increase the WU and SWR to some extent for the melamine-incorporated SWE [28].

3.2. Single-cell performance and durability analysis

The results of the cell performance experiment are presented in Figs. 7 and 8. These investigations were conducted using DI water and brine as feed solutions for comparative analysis. Various concentrations of PVA-KOH-based SWEs were explored with TEAOH and melamine to determine the optimal SWEs for cell performance analysis. The figures demonstrated a continuous increase in current density with rising voltage. Notably, the PVA-TEAOH-KOH SWE exhibited the highest current density across all voltages applied, outperforming both PVA-KOH and M-PVA-TEAOH-KOH SWEs.

In the DI water feed solution, the PVA-TEAOH-KOH-30 wt% SWE achieved a current density of 300 mA cm^{-2} at 2 V, which was higher than the current density of M-PVA-TEAOH-KOH 30 and PVA-KOH 30 wt % SWEs at the same voltage (Fig. 7). In the case of brine, the PVA-TEAOH-KOH-30 wt% SWE reached a current density of 375 mA cm^{-2} at 2 V, significantly higher than that of M-PVA-TEAOH-KOH-30 (251 mA cm^{-2}) and PVA-KOH-30 wt% (321 mA cm^{-2}) (Fig. 8). The higher current density of the PVA-TEAOH-KOH-based SWEs can be attributed to the influence of an alkaline environment due to hydroxide ions from both TEAOH and KOH. Furthermore, TEAOH is a quaternary ammonium salt that dissociates into tetraethylammonium (TEA^+) and hydroxide (OH^-) ions, both of which are relatively mobile and can enhance ion transport within the SWEs. The presence of these ions introduces additional charge carriers, which contributes directly to an increase in ion conductivity [6,16,29,33].

In addition, the WRC, WU and SWR of these SWEs are comparatively higher than PVA-KOH and M-PVA-TEAOH-KOH SWEs (Fig. 6) because TEAOH is highly hygroscopic, meaning it attracts and retains water molecules even in solid or semi-solid materials. When incorporated into a solid electrolyte, TEAOH facilitates water absorption and retention within the electrolyte structure. This retained water can serve as a medium for ion transport, as ions move more readily in hydrated environments than in dry, solid matrices [11,23,24]. The high WRC, WU and SWR of SWE result in the highest water vapor transport through the MD membrane and the subsequent greatest amount of pure water supply to the electrodes-catalysts layers hence increasing current densities and hydrogen production. The reduction in current density observed with the melamine-incorporated SWEs can be explained by reduced ionic conduction due to the restricted movement of ions within the SWE matrix because melamine provides a densely packed and 3-dimensional rigid structure [28,35]. The reduced current density in SWEs with 40 wt % KOH can be linked to a decrease in free water available in the SWEs, as the OH^- ions from KOH interact with the water due to the increased cross-linking density, reduction in polymer solubility and changes of viscosity [34,36].

The higher current densities observed in the brine compared to DI water are likely due to the presence of various ions that increase the electrical conductivity of the feed, which ultimately reduces the ohmic losses and enhances charge transport efficiency. Furthermore, the vapor pressure difference between brine and SWEs is lower compared to DI water and SWEs [37,38]. However, we expected SWEs with 20 wt% of KOH should have a high current density because these SWEs offered the highest ion conductivity (Fig. 6A).

In contrast, PVA-TEAOH-KOH-30 wt% SWE showed the highest cell performance. This could be due to our process design (Fig. 2), where the cell is highly compact, having a direct connection with the brine and MD membrane, facilitating constant water vapor transportation to the SWE chamber, where it was re-liquefied into water molecules. These processes lead to the swelling of the SWEs, which promotes an increase in ion conductivity and the reduction of ion movement resistance. The

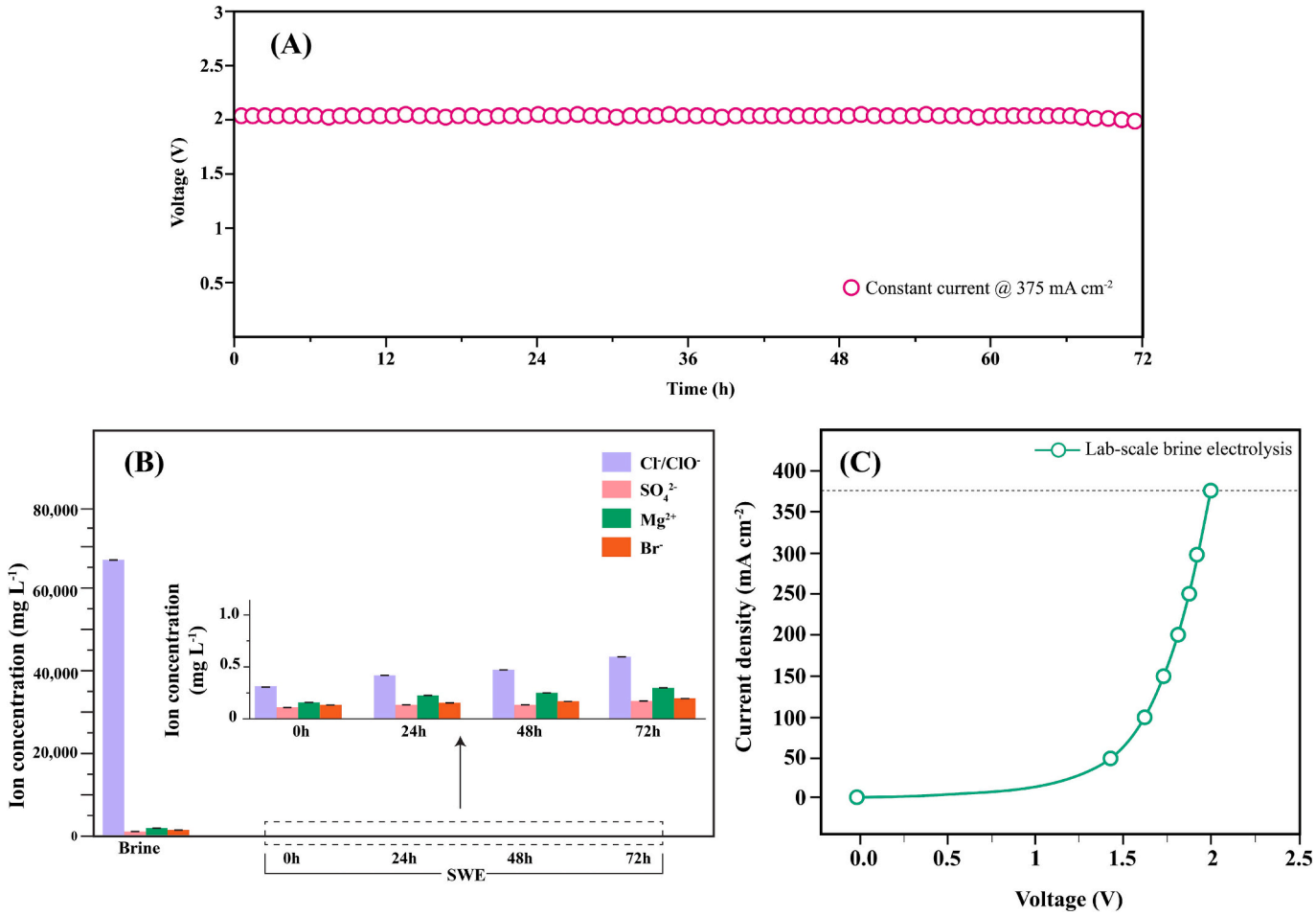

Fig. 9. (A) Chronoamperometry of durability analysis at a constant current density of 375 mA cm^{-2}, (B) ion concentration in brine and SWE at 0 h, 24 h, 48 h and 72 h, and (C) LSV curve of lab-scale brine electrolysis with PVA-TEAOH-KOH-30 wt% SWE.

Table 2
Brine concentrating during long-term electrolysis (72 h).

Remaining brine weight (g)	500	232.12	153.55	56.22[a]
Time (h)	0	24	48	72
Concentration of brine solution (mg/L)	–	–	–	–
EC	17,000 ± 3	24,500 ± 2	36,006 ± 5	51,032 ± 2
TDS	12,000 ± 2	18,234 ± 3	26,340 ± 3	37,320 ± 3
Li^+	100 ± 4	178 ± 4	300 ± 4	645 ± 5
Na^+	33,500 ± 2	35,600 ± 4	40,322 ± 3	41,346 ± 4
K^+	1900 ± 4	2400 ± 5	2920 ± 2	3472 ± 5
Ca^+	5020 ± 7	7345 ± 8	9825 ± 3	13,342 ± 4
Mg^+	400 ± 3	650 ± 2	955 ± 3	1232 ± 3
Cl^-	63,650 ± 1	65,600 ± 2	71,340 ± 6	74,234 ± 1
Br^-	300 ± 2	410 ± 4	644 ± 4	1590 ± 4
SO_4^{-2}	200 ± 3	450 ± 3	867 ± 3	1034 ± 4

[a] 9× concentrated brine.

swelled SWEs provided a significant quantity of water, which is used for the splitting process directed to HER and OER when the water passes through the GDL layers coated with catalysts. We hypothesized that the brine electrolysis process in this study maintained a sustained balance between the migration rate of water vapor through the MD membrane and the re-liquefication rate of the water vapor, which produces pure water inside the SWE chamber. This balanced state of water vapor and water production needed an optimized concentration of KOH in SWEs and, obviously, the vapor pressure difference. Thus, PAV-TEAOH-KOH-30 wt% SWEs secured the highest cell performance and were considered optimized for this process. A comparative study of similar research using saline feed sources in the existing literature and the present study is provided in Table 1, which suggests this process is competitive for impure water electrolysis for a circular economy of hydrogen, oxygen and resources.

The lab-scale durability analysis of the process was conducted at a constant current density of 375 mA cm^{-2} for a period of 72 h to evaluate the cell's stability and performance degradation due to the MD membrane wetting and/or the contamination of SWE during continuous water electrolysis. As shown in Fig. 9A, the voltage remained stable at approximately 2 V throughout the brine electrolysis process, confirming efficient water splitting using the SWE and hydrophobic membrane, and the cell maintained a sustained and robust performance. As shown in Fig. 9B, the ion concentrations in SWE after long-term operation remain significantly lower than the ion concentrations in the original brine. The results indicated that the ion concentration in the SWE remained five orders of magnitude lower than that in the brine after 72 h of electrolysis. Thus, the vapor path in the hydrophobic membrane effectively prevents ion penetration and potential electrode corrosion and side reactions could be avoided in this system to the greatest extent as the concentration of Cl^-/ClO^- and Br^- in SWE is highly insignificant compared to the brine solution [17,24,40]. The trace amounts of ions were observed in the SWE can be attributed to the presence of non-uniform or disproportionate gas-pathway pores within the MD membrane, which may allow only the slightest amount of ion intrusion. However, the presence of these ions does not affect the performance of the electrolysis system. This demonstrates the system's potential for a

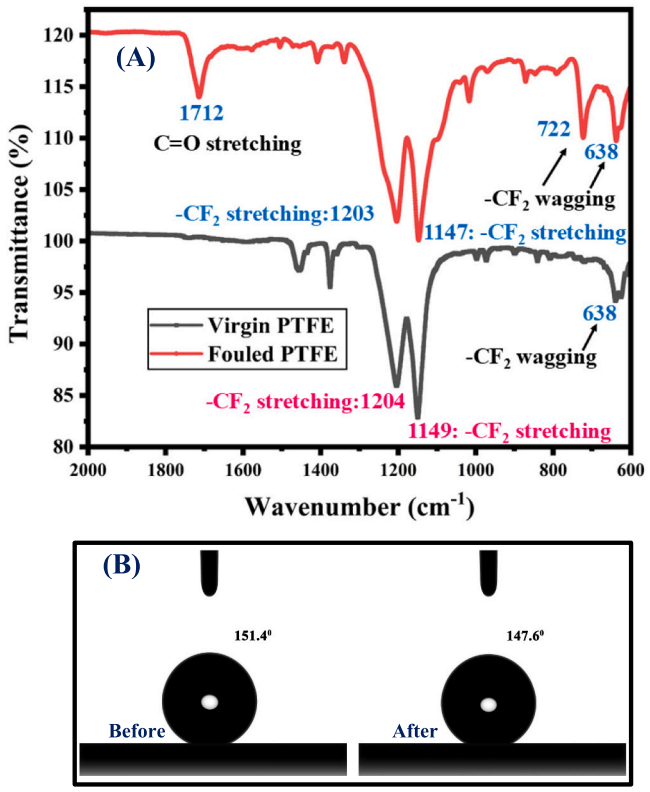

Fig. 10. (A) FTIR spectra of PTFE membrane, (B) contact angle measurement of PTFE membrane after extended brine electrolysis.

prolonged electrolysis application. Additionally, the LSV (Fig. 9C) was performed to determine the onset potential for the hydrogen evolution reaction (HER), which was found to be ~1.5 V, indicating that the HER began significantly at this potential. The composition of concentrated brine after 72 h of electrolysis has been provided in Table 2. The brine was concentrated 9× in volume concentration factor (VCF), which can be a potential source of resources in the downstream processing for a circular economy. The other ions, such as Li^+, Na^+, K^+, Ca^{2+}, Mg^{2+}, and Br^-, were concentrated up to 645, 41,345, 3471, 13,342, 1231 and 1590 mg/L, correspondingly.

3.3. *Investigating the fouling phenomena of MD membrane*

To evaluate the MD membrane fouling phenomena, FTIR analysis was conducted before and after the long-term durability analysis. The FTIR spectrum of the virgin PTFE and the PTFE membrane after 72 h of electrolysis are presented in Fig. 10A.

The virgin PTFE exhibited its characteristic peaks at 1204 and 1149 cm^{-1}, corresponding to the stretching vibrations of the -CF_2 [28], whereas a wagging vibration of -CF_2 was also observed at 638 cm^{-1} [8]. However, there was no significant difference detected in the wavenumber of -CF_2 stretching and -CF_2 wagging peak in the PTFE membrane after electrolysis of brine, but the C═O stretching at 1712 cm^{-1}, indicated organic components. This phenomenon could be attributed to the fact that concentrated brine could potentially cause minor degradation or changes in surface chemistry, possibly leading to the formation of carbonyl groups, although PTFE is quite chemically resistant [16]. Furthermore, the C═O stretching is likely to occur due to the formation of carbonate species ($CaCO_3$). As the brine was synthetic, fouling due to organic contents is unlikely. However, due to the presence of Ca^{+2}, Mg^{+2} and SO_4^{-2} at a high concentration could lead to the formation of carbonate deposits [11]. However, the contact angle measurement also evidently proved that the MD membrane wetting is insignificant after long-term brine electrolysis compared to the virgin membranes (Fig. 10B).

To cross-check the fouling issue further, FESEM-EDX has been analyzed and represented in Fig. 11. The FESEM micrographs revealed that both virgin PTFE and PTFE membranes after 72 h of electrolysis had almost similar rough, irregular, and unsymmetrical surface structures. However, we noticed some random whitish appearances in the fouled PTFE membrane that could be due to the carbonate scaling from inorganic constituents present in the brine [11,16], which is also supported by the FTIR analysis. The EDX analysis highlights a slight decrease in carbon and fluorine content in the fouled membrane, which could indicate partial surface degradation or the masking of PTFE by the foulants. The ultra-trace level presence of Na^+, K^+, Ca^{2+} and Mg^{2+} on the fouled membrane suggests that inorganic salts from the brine were involved in the scaling process, confirmed by FESEM and FTIR [8].

4. Conclusion

This study presents a novel electrolyzer designed to integrate hydrogen production and resource recovery within a circular economy framework. The core innovation lies in the integration of advanced solid electrolytes functioning as self-wetted electrolytes (SWEs) with membrane distillation (MD) facilities, enabling a two-step brine electrolysis process. Notably, this electrolyzer eliminates the need for brine pretreatment, thereby reducing the overall energy consumption and lowering hydrogen production costs. Additionally, the recirculated concentrated brine and produced oxygen support the future hydrogen economy by effectively closing the resources and energy loops.

The incorporation of tetraethylammonium hydroxide (TEAOH) into the SWE significantly improved its dimensional and electrochemical stability. These enhancements are vital for maintaining a continuous supply of pure water at the electrode-catalyst interface, ensuring efficient water splitting for hydrogen generation. The PVA-TEAOH-KOH-30 wt% SWE demonstrated the highest ion conductivity (112.4 mS cm^{-1}), achieving excellent cell performance with a current density of 375 mA cm^{-2}. Lab-scale durability testing over 72 h revealed robust performance, with the brine concentration increasing ninefold in volume concentration factor (VCF) without significant wetting of the MD membrane, as confirmed through chronoamperometry and linear sweep voltammetry (LSV).

This electrolyzer offers significant advantages over conventional alkaline electrolyte systems, including reduced electrode corrosion, minimal undesirable side reactions, and lower gas cross-over risks. These benefits are attributed to the dramatic reduction in Cl^-/ClO^-, Br^-, and other ion concentrations in the SWE, which was reduced by five orders of magnitude compared to the original brine. The hydrogen produced serves as a clean energy source, while oxygen finds applications as a pure, breathable supply and in various industrial processes. Furthermore, the concentrated brine can be processed into valuable resources for industries such as chloro-alkali, chemicals, cement, food, fertilizers, pharmaceuticals, and batteries, to name but a few.

Overall, this technology offers a sustainable solution to future energy challenges, with the potential to transform the hydrogen and oxygen economies while promoting a circular economy through efficient resource recovery. Its application is particularly promising in regions with limited continuous electricity supply and scarce freshwater resources, such as deserts, remote islands, and densely populated urban centers.

However, scaling up this technology requires further optimization of the SWE to enhance ion conductivity, thermal resistance, and long-term durability. Furthermore, improving the morphological and electrochemical properties of the hydrophobic MD membrane could significantly enhance the cell performance while effectively controlling the ion migration in the self-wetted electrolytes. Comprehensive system durability testing, including assessments of MD membrane performance under extended operation, is crucial to ensure the system's reliability.

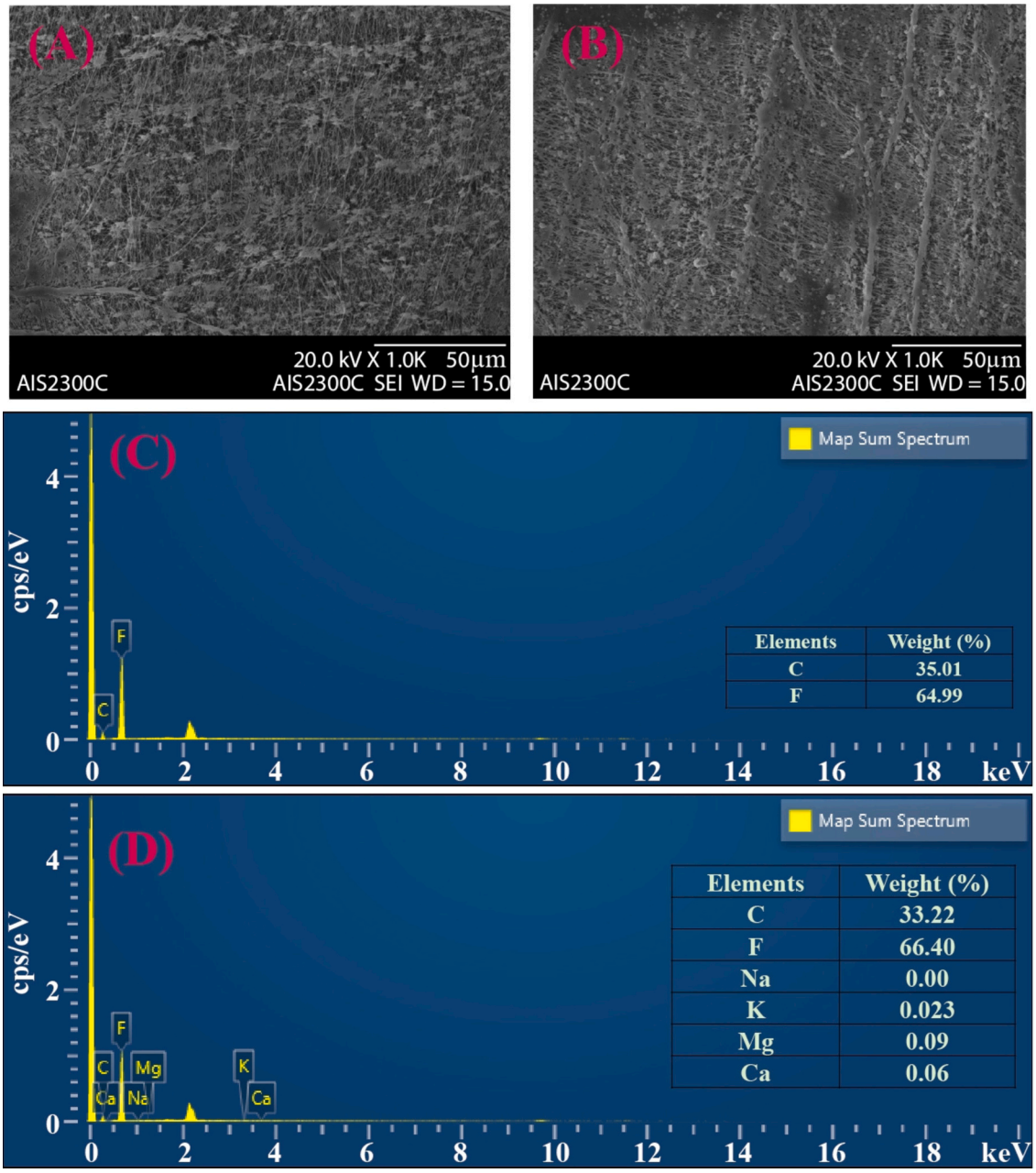

Fig. 11. FESEM micrographs and EDX results of PTFE membrane after long-term brine electrolysis. (A) Virgin PTFE membrane, (B) fouled PTFE membrane, (C) EDX spectra of virgin PTFE membrane and (D) EDX spectra of fouled PTFE membrane.

Future endeavors to assess the feasibility of this technology using real seawater and brine will extend its applicability. Additionally, a detailed techno-economic and environmental sustainability analysis is essential to evaluate its feasibility and potential impact at a commercial scale.

CRediT authorship contribution statement

Mohammad Mahbub Kabir: Conceptualization, Data curation, Formal analysis, Investigation, Writing – original draft. **Kwang Seop Im:** Investigation. **Leonard Tijing:** Investigation, Project administration, Supervision, Validation, Writing – review & editing. **Yeshi Choden:** Investigation, Validation, Writing – review & editing. **Sherub Phuntsho:** Funding acquisition, Investigation, Project administration, Supervision, Writing – review & editing. **Md. Fazlul Karim Mamun:** Formal analysis, Investigation, Writing – review & editing. **Golam Md. Sabur:** Data curation, Formal analysis, Investigation, Writing – review & editing. **Sang Yong Nam:** Supervision, Validation, Writing – review & editing. **Ho Kyong Shon:** Conceptualization, Data curation, Formal analysis, Funding acquisition, Investigation, Project administration, Resources, Supervision, Validation, Writing – review & editing.

Declaration of competing interest

The authors declare no conflict of interest reported in this paper. Ho Kyong Shon serves as a Co-Editor-In-Chief for the Desalination journal, while the editorial handling and review of this manuscript were overseen by a different Co-Editor-In-Chief.

Acknowledgements

The research reported in this paper was supported by the Australian Research Council (ARC) Industrial Transformation Research Hub on

Nutrients in a Circular Economy (NiCE) (IH210100001). This research was also supported by the Basic Science Research Program through the National Research Foundation of Korea (NRF), funded by the Ministry of Education (2020R1A6A03038697). Mohammad Mahbub Kabir would like to acknowledge the financial support from the University of Technology Sydney (UTS) through the UTS President Scholarship (UTSP), International Research Scholarship (IRS), UTS Faculty of Engineering and IT Top-up scholarship and an Industrial Transformation Research Hub Top-up scholarship during his PhD study.

Appendix A. Supplementary data

Supplementary data to this article can be found online at https://doi.org/10.1016/j.desal.2025.118580.

Data availability

No data was used for the research described in the article.

References

[1] M.M. Kabir, M.M. Akter, Z. Huang, L. Tijing, H.K. Shon, Hydrogen production from water industries for a circular economy, Desalination (2023) 554, https://doi.org/10.1016/j.desal.2023.116448.
[2] M.M. Akter, I.Z. Surovy, N. Sultana, M.O. Faruk, B.H. Gilroyed, L. Tijing, et al., Techno-economics and environmental sustainability of agricultural biomass-based energy potential, Appl. Energy (2024) 359, https://doi.org/10.1016/j.apenergy.2024.122662.
[3] M.M. Kabir, G.M. Sabur, M.M. Akter, S.Y. Nam, K.S. Im, L. Tijing, et al., Electrodialysis desalination, resource and energy recovery from water industries for a circular economy, Desalination (2024) 569, https://doi.org/10.1016/j.desal.2023.117041.
[4] M.M. Kabir, S.K. Roy, F. Alam, S.Y. Nam, K.S. Im, L. Tijing, et al., Machine learning-based prediction and optimization of green hydrogen production technologies from water industries for a circular economy, Desalination (2023) 567, https://doi.org/10.1016/j.desal.2023.116992.
[5] A. Das, K.S. Im, M.M. Kabir, H.K. Shon, S.Y. Nam, Polybenzimidazole (PBI)-based membranes for fuel cell, water electrolysis and desalination, Desalination (2024) 579, https://doi.org/10.1016/j.desal.2024.117500.
[6] K. Im, M. Park, M.M. Kabir, W. Sohn, Y. Choo, H.K. Shon, et al., Human urine electrolysis for simultaneous green hydrogen and liquid fertilizer production for a circular economy: a proof of concept, Desalination (2024) 570, https://doi.org/10.1016/j.desal.2023.117059.
[7] J.N. Hausmann, R. Schlögl, P.W. Menezes, M. Driess, Is direct seawater splitting economically meaningful? Energy Environ. Sci. 14 (2021) 3679–3685, https://doi.org/10.1039/d0ee03659e.
[8] M. Paidar, V. Fateev, K. Bouzek, Membrane electrolysis—history, current status and perspective, Electrochim. Acta 209 (2016) 737–756, https://doi.org/10.1016/j.electacta.2016.05.209.
[9] R.R. Beswick, A.M. Oliveira, Y. Yan, Does the green hydrogen economy have a water problem? ACS Energy Lett. 6 (2021) 3167–3169, https://doi.org/10.1021/acsenergylett.1c01375.
[10] J. Zhang, W. Hu, S. Cao, L. Piao, Recent progress for hydrogen production by photocatalytic natural or simulated seawater splitting, Nano Res. 13 (2020) 2313–2322, https://doi.org/10.1007/s12274-020-2880-z.
[11] X. Zhang, W. Zhao, Y. Zhang, V. Jegatheesan, A review of resource recovery from seawater desalination brine, Rev. Environ. Sci. Biotechnol. 20 (2021) 333–361, https://doi.org/10.1007/s11157-021-09570-4.
[12] T. Liu, Z. Zhao, W. Tang, Y. Chen, C. Lan, L. Zhu, et al., In-situ direct seawater electrolysis using floating platform in ocean with uncontrollable wave motion, Nat. Commun. (2024) 15, https://doi.org/10.1038/s41467-024-49639-6.
[13] J. Guo, Y. Zheng, Z. Hu, C. Zheng, J. Mao, K. Du, et al., Direct seawater electrolysis by adjusting the local reaction environment of a catalyst, Nat. Energy 8 (2023) 264–272, https://doi.org/10.1038/s41560-023-01195-x.
[14] Y. Zhao, Z. Yu, A. Ge, L. Liu, J.L. Faria, G. Xu, et al., Direct seawater splitting for hydrogen production: recent advances in materials synthesis and technological innovation, Green Energy and Environment (2024), https://doi.org/10.1016/j.gee.2024.02.001.
[15] S.S. Veroneau, D.G. Nocera, C.P. Berlinguette, D.V. Esposito, M. Koper, Continuous Electrochemical Water Splitting From Natural Water Sources via Forward Osmosis, 2021, https://doi.org/10.1073/pnas.2024855118/-/DCSupplemental.
[16] H. Xie, Z. Zhao, T. Liu, Y. Wu, C. Lan, W. Jiang, et al., A membrane-based seawater electrolyser for hydrogen generation, Nature 612 (2022) 673–678, https://doi.org/10.1038/s41586-022-05379-5.
[17] M.E.H. Bergmann, T. Iourtchouk, W. Schmidt, J. Hartmann, M. Fischer, G. Nüsske, et al., Laboratory- and technical-scale comparison of chlorate and perchlorate formation during drinking water electrolysis: a field study, J. Appl. Electrochem. 45 (2015) 765–778, https://doi.org/10.1007/s10800-015-0826-z.
[18] L. Fan, J. Chen, G. Qin, L. Wang, X. Hu, Z. Shen, Preparation of PVA-KOH-halloysite nanotube alkaline solid polymer electrolyte and its application in Ni-MH battery, Int. J. Electrochem. Sci. 12 (2017) 5142–5156, https://doi.org/10.20964/2017.06.65.
[19] K. Shi, H. Wan, K. Wang, F. Fang, S. Li, Y. Wang, et al., Self-sustaining alkaline seawater electrolysis via forward osmosis membranes, Green Energy and Environment (2024), https://doi.org/10.1016/j.gee.2024.04.003.
[20] Y. Kuang, M.J. Kenney, Y. Meng, W.H. Hung, Y. Liu, J.E. Huang, et al., Solar-driven, highly sustained splitting of seawater into hydrogen and oxygen fuels, Proc. Natl. Acad. Sci. USA 116 (2019) 6624–6629, https://doi.org/10.1073/pnas.1900556116.
[21] F. Sun, J. Qin, Z. Wang, M. Yu, X. Wu, X. Sun, et al., Energy-saving hydrogen production by chlorine-free hybrid seawater splitting coupling hydrazine degradation, Nat. Commun. (2021) 12, https://doi.org/10.1038/s41467-021-24529-3.
[22] S. Dresp, T. Ngo Thanh, M. Klingenhof, S. Brückner, P. Hauke, P. Strasser, Efficient direct seawater electrolysers using selective alkaline NiFe-LDH as OER catalyst in asymmetric electrolyte feeds, Energy Environ. Sci. 13 (2020) 1725–1729, https://doi.org/10.1039/d0ee01125h.
[23] P. Kumar, A. Date, N. Mahmood, R. Kumar Das, B. Shabani, Freshwater supply for hydrogen production: An underestimated challenge, Int. J. Hydrog. Energy 78 (2024) 202–217, https://doi.org/10.1016/j.ijhydene.2024.06.257.
[24] R. Asiain-Mira, C. Smith, P. Zamora, V.M. Monsalvo, L. Torrente-Murciano, Hydrogen production from urea in human urine using segregated systems, Water Res. (2022) 222, https://doi.org/10.1016/j.watres.2022.118931.
[25] W.X. Waresindo, H.R. Luthfianti, A. Priyanto, D.A. Hapidin, D. Edikresnha, A. H. Aimon, et al., Freeze–thaw hydrogel fabrication method: basic principles, synthesis parameters, properties, and biomedical applications, Mater Res Express 10 (2023) 024003, https://doi.org/10.1088/2053-1591/ACB98E.
[26] Hu L, Wrubel JA, Baez-Cotto CM, Intia F, Park JH, Kropf AJ, et al. A scalable membrane electrode assembly architecture for efficient electrochemical conversion of CO2 to formic acid. Nature Communications 2023 14:1 2023;14:1–11. doi:https://doi.org/10.1038/s41467-023-43409-6.
[27] Kumar A. Reena, V. Mahto, A.K. Choubey, Synthesis and characterization of cross-linked hydrogels using polyvinyl alcohol and polyvinyl pyrrolidone and their blend for water shut-off treatments, J. Mol. Liq. (2020) 301, https://doi.org/10.1016/j.molliq.2020.112472.
[28] H. Liao, Y. Liu, Q. Wang, W. Duan, Preparation and properties of a poly(vinyl alcohol) hydrogel-melamine formaldehyde foam composite, Polym. Compos. 40 (2019) 2067–2075, https://doi.org/10.1002/pc.24988.
[29] J. Li, J. Qiao, K. Lian, Hydroxide ion conducting polymer electrolytes and their applications in solid supercapacitors: a review, Energy Storage Mater 24 (2020) 6–21, https://doi.org/10.1016/j.ensm.2019.08.012.
[30] Li X, Zhao L, Yu J, Liu X, Zhang X, Liu H, et al. Water splitting: from electrode to green energy system. Nano-Micro Letters 2020 12:1 2020;12:1–29. doi:https://doi.org/10.1007/S40820-020-00469-3.
[31] X. Xia, L. Wang, N. Sui, V.L. Colvin, W.W. Yu, Recent progress in transition metal selenide electrocatalysts for water splitting, Nanoscale 12 (2020) 12249–12262, https://doi.org/10.1039/D0NR02939D.
[32] É. Lucas, L. Han, I. Sullivan, H.A. Atwater, C. Xiang, Measurement of ion transport properties in ion exchange membranes for photoelectrochemical water splitting, Front Energy Res 10 (2022) 1001684, https://doi.org/10.3389/FENRG.2022.1001684/BIBTEX.
[33] Qu S, Liu B, Fan X, Liu X, Liu J, Ding J, et al. 3D foam anode and hydrogel electrolyte for high-performance and stable flexible zinc–air battery. ChemistrySelect 2020;5:8305–10. doi:https://doi.org/10.1002/slct.202002573.
[34] Z. Yu, L. Liu, Recent advances in hybrid seawater electrolysis for hydrogen production, Adv. Mater. (2024) 36, https://doi.org/10.1002/adma.202308647.
[35] C. Lei, C. Ji, H. Mi, C. Yang, Q. Zhang, S. He, et al., Engineering kinetics-favorable carbon sheets with an intrinsic network for a superior supercapacitor containing a dual cross-linked hydrogel electrolyte, ACS Appl. Mater. Interfaces 12 (2020) 53164–53173, https://doi.org/10.1021/acsami.0c16985.
[36] X. Lu, J. Pan, E. Lovell, T.H. Tan, Y.H. Ng, R. Amal, A sea-change: manganese doped nickel/nickel oxide electrocatalysts for hydrogen generation from seawater, Energy Environ. Sci. 11 (2018) 1898–1910, https://doi.org/10.1039/c8ee00976g.
[37] X. Du, M. Tan, T. Wei, H. Kobayashi, J. Song, Z. Peng, et al., Highly efficient and robust nickel-iron bifunctional catalyst coupling selective methanol oxidation and freshwater/seawater hydrogen evolution via CO-free pathway, Chem. Eng. J. 452 (2023) 139404, https://doi.org/10.1016/j.cej.2022.139404.
[38] J. Mohammed-Ibrahim, H. Moussab, Recent advances on hydrogen production through seawater electrolysis, Mater Sci Energy Technol 3 (2020) 780–807, https://doi.org/10.1016/j.mset.2020.09.005.
[39] Z. Yu, Y. Li, V. Martin-Diaconescu, L. Simonelli, J.R. Esquius, I. Amorim, et al., Highly efficient and stable saline water electrolysis enabled by self-supported nickel-iron phosphosulfide nanotubes with heterointerfaces and under-coordinated metal active sites, Adv. Funct. Mater. 32 (2022) 2206138, https://doi.org/10.1002/adfm.202206138.
[40] Z. Yu, J. Xu, L. Meng, L. Liu, Efficient hydrogen production by saline water electrolysis at high current densities without the interfering chlorine evolution, J Mater Chem A Mater (2021) 22248–22253, https://doi.org/10.1039/D1TA05703K.
[41] X. Jia, H. Kang, G. Hou, W. Wu, S. Lu, Y. Li, et al., Coupling ferricyanide/ferrocyanide redox mediated recycling spent LiFePO4 with hydrogen production, Angew. Chem. 136 (2024) e202318248, https://doi.org/10.1002/ange.202318248.
[42] Y. Yang, R. Zou, J. Gan, Y. Wei, Z. Chen, X. Li, et al., Integrating electrocatalytic seawater splitting and biomass upgrading via bifunctional nickel cobalt phosphide

nanorods, Green Chem. 25 (2023) 4104–4112, https://doi.org/10.1039/D3GC00684K.
[43] B. Kim, H.K. Shon, D.S. Han, H. Park, In-situ desalination-coupled electrolysis with concurrent one-step-synthesis of value-added chemicals, Desalination 551 (2023) 116431, https://doi.org/10.1016/j.desal.2023.116431.
[44] G.S. Cassol, C. Shang, A.K. An, N.K. Khanzada, F. Ciucci, A. Manzotti, et al., Ultra-fast green hydrogen production from municipal wastewater by an integrated forward osmosis-alkaline water electrolysis system, Nat. Commun. (2024) 15, https://doi.org/10.1038/s41467-024-46964-8.
[45] S.S. Veroneau, D.G. Nocera, C.P. Berlinguette, D.V. Esposito, M. Koper, Continuous electrochemical water splitting from natural water sources via forward osmosis, Proc. Natl. Acad. Sci. USA (2024), https://doi.org/10.1073/pnas.2024855118/-/DCSupplemental.
[46] D. Chauhan, Y.H. Ahn, Alkaline electrolysis of wastewater and low-quality water, J. Clean. Prod. (2023) 397, https://doi.org/10.1016/j.jclepro.2023.136613.